doi:10.1093/brain/aws193 Brain 2012: 135; 2750–2765 | 2750

BRAIN
A JOURNAL OF NEUROLOGY

Late-onset Parkinsonism in NFκB/c-Rel-deficient mice

Cristina Baiguera,[1] Manuela Alghisi,[1] Annalisa Pinna,[2,3] Arianna Bellucci,[1] Maria Antonietta De Luca,[3] Lucia Frau,[2,3] Micaela Morelli,[2,3] Rosaria Ingrassia,[1] Marina Benarese,[1] Vanessa Porrini,[1] Michele Pellitteri,[4] Giuseppe Bertini,[4] Paolo Francesco Fabene,[4] Sandra Sigala,[1] Maria Grazia Spillantini,[5] Hsiou-Chi Liou,[6] Pier Franco Spano[1,7] and Marina Pizzi[1,7]

1 Department of Biomedical Sciences and Biotechnologies, University of Brescia and National Institute of Neuroscience, 25123 Brescia, Italy
2 National Research Council, Institute of Neuroscience, 09124 Cagliari, Italy
3 Department of Biomedical Science and National Institute of Neuroscience, University of Cagliari, 09124 Cagliari, Italy
4 Department of Neurological, Neuropsychological, Morphological and Motor Sciences, University of Verona, 37134 Verona, Italy
5 Department of Clinical Neurosciences, Brain Repair Centre, University of Cambridge, Forvie Site, Robinson Way, Cambridge, CB2 0PY, UK
6 Department of Immunology, Weill Medical College of Cornell University, New York, 10065 NY, USA
7 IRCCS San Camillo Hospital, Venice, Italy

Correspondence to: Marina Pizzi
Department of Biomedical Sciences and Biotechnologies
Viale Europa, 11
25123 Brescia, Italy
E-mail: pizzi@med.unibs.it

Activation of the nuclear factor κB/c-Rel can increase neuronal resilience to pathological noxae by regulating the expression of pro-survival manganese superoxide dismutase (*MnSOD*, now known as *SOD2*) and Bcl-xL genes. We show here that c-Rel-deficient (c-rel$^{-/-}$) mice developed a Parkinson's disease-like neuropathology with ageing. At 18 months of age, c-rel$^{-/-}$ mice exhibited a significant loss of dopaminergic neurons in the substantia nigra pars compacta, as assessed by tyrosine hydroxylase-immunoreactivity and Nissl staining. Nigral degeneration was accompanied by a significant loss of dopaminergic terminals and a significant reduction of dopamine and homovanillic acid levels in the striatum. Mice deficient of the c-Rel factor exhibited a marked immunoreactivity for fibrillary α-synuclein in the substantia nigra pars compacta as well as increased expression of divalent metal transporter 1 (*DMT1*) and iron staining in both the substantia nigra pars compacta and striatum. Aged c-rel$^{-/-}$ mouse brain were characterized by increased microglial reactivity in the basal ganglia, but no astrocytic reaction. In addition, c-rel$^{-/-}$ mice showed age-dependent deficits in locomotor and total activity and various gait-related deficits during a catwalk analysis that were reminiscent of bradykinesia and muscle rigidity. Both locomotor and gait-related deficits recovered in c-rel$^{-/-}$ mice treated with L-3,4-dihydroxyphenylalanine. These data suggest that c-Rel may act as a regulator of the substantia nigra pars compacta resilience to ageing and that aged c-rel$^{-/-}$ mice may be a suitable model of Parkinson's disease.

Keywords: Parkinson's disease; NFκB/c-Rel; α-synuclein; motor impairments; L-DOPA

Abbreviations: ChAT = choline acetyl transferase; GFAP = glial fibrillary acidic protein; MPTP = 1-methyl-4-phenyl-1,2,3, 6-,tetrahydropyridine

Received December 07, 2011. Revised May 14, 2012. Accepted June 6, 2012. Advance Access publication August 21, 2012

Introduction

Parkinson's disease is the most common neurodegenerative movement disorder, with clinical symptoms that include resting tremor, rigidity and bradykinesia (Fahn, 2003). The aetiology of Parkinson's disease is not well understood but it is likely that it involves both genetic and environmental factors (Wirdefeldt *et al.*, 2011). The pathological hallmarks of Parkinson's disease are the loss of dopamine neurons in the pars compacta of the substantia nigra and the accumulation of somatic and intraneuritic inclusions, which are mainly composed of filamentous α-synuclein aggregates called Lewy bodies and Lewy neurites, respectively (Spillantini *et al*., 1998; Bellucci *et al*., in press). Furthermore, the activation of microglia and neuroinflammatory changes (Hirsch and Hunot, 2009), accumulation of iron with its transporter, the divalent metal transporter 1 (*DMT1*) (Salazar *et al.*, 2008), are found in the Parkinson's disease brain.

In post-mortem Parkinson's disease brains, affected dopaminergic neurons display morphological characteristics of apoptosis, including cell shrinkage, chromatin condensation and DNA fragmentation (Olanow and Tatton, 1999; Dauer and Przedborski, 2003). To date, the mechanisms underlying the progressive loss of dopamine neurons in Parkinson's disease remain unknown. NFκB is a cardinal transcriptional regulator of inflammation and apoptosis that can contribute to the pathological processes associated with neurodegeneration (Pizzi and Spano, 2006; Camandola and Mattson, 2007). NFκB is activated in the neurons of brains exposed to trauma or ischaemia (Bethea *et al*., 1998; Schneider *et al*., 1999), as well as in the brains of patients affected by Parkinson's disease (Hunot *et al*., 1997; Ghosh *et al*., 2007) and Alzheimer's disease (Kaltschmidt *et al*., 1997). Of note, conflicting evidence has emerged regarding the pro-apoptotic or anti-apoptotic pathway activated by NFκB in neurons (Pizzi and Spano, 2006; Camandola and Mattson, 2007). We recently showed that the subunit composition of the NFκB dimer is essential to define the pro- or anti-apoptotic activity of this factor. Five DNA-binding proteins [p50, p52, p65 (RelA), c-Rel and RelB] can compose the NFκB complexes, and targeting RelA or c-Rel expression revealed opposing regulation of neuron survival. The RelA subunit within the activated p50/RelA dimer plays a pivotal role in the onset of neurodegenerative processes triggered by ischaemic insults or glutamate and amyloid-β toxicity (Pizzi *et al*., 2002, 2005; Inta *et al*., 2006) and activates the transcription of pro-apoptotic *Bim* (now known as *Bcl2l11*) and *Noxa* (now known as *Pmaip1*) genes (Inta *et al*., 2006). Conversely, the c-Rel subunit within activated NFκB dimer counteracts the ischaemic injury (Sarnico *et al*., 2009) and is responsible for neuroprotection elicited by IL1β, mGlu5 agonists or leptin (Pizzi *et al*., 2002, 2005; Valerio *et al*., 2009). Over-expression of c-Rel in cultured neurons promotes anti-apoptotic effects by inducing the transcription of manganese superoxide dismutase (*MnSOD*, now known as *SOD2*) and Bcl-xL (Chen *et al*., 2000; Bernard *et al*., 2001; Pizzi *et al*., 2005; Sarnico *et al*., 2009). Over-expression of c-Rel also limits the generation of reactive oxygen species by inducing transcription of the mitochondrial uncoupling proteins 4 (*UCP4*) (Ho *et al*., 2012), a brain-specific mitochondrial ion channel producing mild reduction of mitochondrial membrane potential and neuroprotection (Echtay, 2007). Knocking down c-Rel expression with RNA interference suppresses the pro-survival effects of NFκB and increases neuronal susceptibility to brain ischaemia (Sarnico *et al*., 2009). This evidence, in addition to the demonstration that c-rel$^{-/-}$ mice display deficits in spatial memory formation, long-term potentiation and long-term depression of hippocampal synaptic transmission (Levenson *et al*., 2004; O'Riordan *et al*., 2006; Ahn *et al*., 2008), indicates a peculiar role for c-Rel in the regulation of fundamental brain functions, such as resilience to stressful conditions and cognition.

In this study, our working hypothesis was that the c-Rel protein might play a role in neurological conditions associated with neuronal cell loss and that changes in c-Rel expression might contribute to neuronal vulnerability in age-related neurodegeneration. In line with this hypothesis, we investigated the occurrence of pathological changes in c-rel-deficient mice that may be associated with changes occurring in Parkinson's disease. We found that aged c-rel$^{-/-}$ mice developed Parkinson's disease-like degeneration of substantia nigra pars compacta characterized by a loss of dopaminergic neurons, increased levels of iron and DMT1, as well as an accumulation of aggregated α-synuclein with activation of microglial cells. In addition, c-rel$^{-/-}$ mice showed motor deficits similar to Parkinson's disease-like hypokinesia, suggesting that they may represent a valuable model of parkinsonism.

Materials and methods

Experimental animals

C57BL/6 mice carrying the *c-Rel* gene null mutation (c-rel$^{-/-}$) were originally generated by inserting the neomycin cassette into the fifth exon of the *c-Rel* gene (Liou *et al*., 1999). The c-rel$^{-/-}$ mice were backcrossed to C57BL/6J mice for nine generations before being used in this study. The genotypes were verified by PCR analysis (wild-type c-rel forward primer, 5′-AAGTGGGGTTACAGGTGCTCA-3′; wild-type c-rel reverse primer, 5′-TTGCCAATAGGCTTAGTCAAATA-3′; c-rel neomycin reverse primer, 5′-CTCTCGTGGGATCATTGTTTTTC-3′). PCR conditions were 94°C for 30 s, 57°C for 30 s, 72° for 30 s (30 cycles). The c-rel$^{-/-}$ and c-rel$^{+/+}$ (wild-type) lines were continued by homozygous breeding. Animals were housed in standard cages and maintained under a 12h/12h light:dark cycle with food and water available *ad libitum*. Humidity was kept at a constant level, and the room temperature was maintained at 22–23°C. All animal experiments were authorized by the Italian Ministry of Health and by the University of Brescia Animal Care Committee in compliance with the Italian guidelines for animal care (DL 116/92) and the European Communities Council Directive (86/609/EEC).

Immunohistochemistry

Mice were anaesthetized with chloral hydrate (400 mg/kg intraperitoneally) and transcardially perfused with PBS (SIGMA), 4% (w/v) ice-cold paraformaldehyde and 14% (w/v) ice-cold picric acid (SIGMA). Coronal slices (30 or 10 μm thickness) were cut to obtain serial sections of the following cerebral areas using bregma-based coordinates (Franklin and Paxinos, 2008): substantia nigra pars compacta (anterior–posterior −2.54 to −3.40 mm), ventral tegmental area

(anterior–posterior −2.92 to −3.80 mm), medial septal area (anterior–posterior 1.18 to 0.38 mm), nucleus basalis magnocellularis (anterior–posterior −0.34 to −1.34 mm) and striatum (anterior–posterior 1.70 to −2.30 mm).

3,3′-Diaminobenzidene immunostaining was performed on free-floating sections (30 μm) using primary antibodies: rabbit polyclonal anti-tyrosine hydroxylase (1:400 Millipore); polyclonal anti-choline acetyl transferase (ChAT; 1:500 Chemicon); mouse monoclonal anti-neuronal nuclei antibody (NeuN; clone A60, 1:100 Millipore); anti-α-synuclein antibody (Syn-1, 1:500 BD); monoclonal mouse anti-glial fibrillary acidic protein (GFAP; 1:400, Sigma); monoclonal rat anti-mouse CD11b (1:1000, Serotec). Brain sections were incubated in biotinylated secondary antibodies (all purchased from Vector) and visualized by avidin–biotin–horseradish peroxidase technique (ABC Elite; Vector Laboratories) using 0.025% 3,3′-diaminobenzidine (Sigma) as the chromogen. NeuN staining was intensified by adding 0.02% $NiCl_2$ to 3,3′-diaminobenzidine solution.

The double tyrosine hydroxylase staining was performed by incubating the sections previously processed for α-synuclein immunoreactivity in the anti-tyrosine hydroxylase antibody and biotinylated secondary antibody (goat anti-rabbit 1:250 Dako) followed by the avidin–biotin–horseradish peroxidase complex and SG reagent as chromogen.

For ferric iron, a Prussian blue stain with diaminobenzidine enhancement was used (Smith *et al*., 1997). Sections were incubated with 7% potassium ferrocyanide (Perls reagent) in 3% HCl for 1 h at 37°C followed by distilled water and 0.015% H_2O_2-activated 0.75 mg/ml diaminobenzidine in 0.1 M PBS for 10 min.

Nissl staining of substantia nigra pars compacta was performed by incubating the sections (10-μm thick) in 0.5% cresyl violet (Sigma-Aldrich). Sections were dehydrated and defatted in xylene and mounted with Eukitt (Calibrated Instruments).

Double immunofluorescence staining was performed in sections (10 μm) incubated with α-synuclein antibody overnight at 4°C followed by a goat anti-mouse secondary antibody conjugated with Cy3 (1:400 Jackson ImmunoResearch) for 30 min at room temperature. Slices were then incubated with a primary rabbit anti-tyrosine hydroxylase (1:200 Chemicon) antibody overnight at 4°C followed by incubation in Alexa Fluor® 405-conjugated secondary antibodies (1:400 Jackson ImmunoResearch). For thioflavin S/α-synuclein double staining, sections were incubated with 0.3% $KMnO_4$ for 3–5 min, washed with water and incubated with a solution of 0.1% $NaBH_4$ for 5 min and then placed in a high-concentration PO_4 buffer (411 mM NaCl, 8.1 mM KCl, 30 mM $NaHPO_4$, 5.2 mM KH_2PO_4) pH 7.2. After washing, thioflavin S (Sigma-Aldrich) and α-synuclein immunostaining was performed and the sections examined with a Zeiss, LSM 510 META confocal microscope (Carl Zeiss), with the laser set at λ = 405–488–543 nm and the height of the section scanning = 1 mm. Images (512 × 512 pixels) were then re-constructed using LSM Image Examiner (Carl Zeiss) and Adobe Photoshop® 7.0 software.

Cell quantification

The number of tyrosine hydroxylase-, ChAT- and NeuN- immunopositive or Nissl-stained cells was stereologically estimated by double-blind cell counting in bright field microscopy using an optical fractionator method (King *et al*., 2002). Neurons from the substantia nigra pars compacta, ventral tegmental area, basal forebrain and striatum were analysed with an inverted microscope (Zeiss Axiovert S100 and camera PCO Sensicam) interfaced with a PC running the StagePro module of Image-Pro™ Plus software (version 6.2, Media Cybernetics, Inc.) as previously described (King *et al*., 2002). The entire extension of mesencephalon, basal forebrain and striatum were cut into sections. Three sections (30 μm thick) were examined every 150 μm in a rostro-caudal extension. In the mesencephalon, tyrosine hydroxylase-immunoreactive cells lateral to the medial terminal nucleus of the accessory optic tract, which defines the medial border of the substantia nigra pars compacta were counted. The ventral tegmental area was thereby excluded from these cell counts. Tyrosine hydroxylase-positive cells in the ventral tegmental area were counted in a separate analysis. Nissl-stained neurons in the substantia nigra were examined in two sections (10 μm thick) every 150 μm.

The number of cholinergic neurons in the basal forebrain was determined by counting ChAT-positive cells in the medial septal area and in the nucleus basalis magnocellularis. For the striatum, NeuN-positive cells with identifiable nuclei were counted in three regions selected between lateral ±1.00 to ±2.00 mm and ventral ±2.00 to ±3.00 mm, (520 × 380 μm; left and right). Values are expressed as the mean ± SEM.

The optical density of striatal tyrosine hydroxylase-positive fibres was examined from digitized images using Image-Pro® Plus software (version 6.2, Media Cybernetics). Brains from four mice (three sections from each mouse) were analysed by examining an average of 10 fields per section.

Quantification of CD11b- and glial fibrillary acidic protein-positive cells

Quantification of CD11b and GFAP immunostaining was carried out in brain slices sections processed on the same day in order to avoid any difference in staining intensity among animals. All pictures were captured within the same session in order to avoid any difference in any differences in lighting conditions. In each section, the entire left and right substantia nigra pars compacta were analysed, whereas for the striatum evaluation, one portion from the dorsolateral striatum (lateral from ±1.65 to ±2.15; ventral from −2.00 to −2.40) and one from the ventromedial striatum (lateral from ±1.25 to ±1.75; ventral from −1.75 to −2.15, 520 × 380 μm; left and right) were analysed. For each animal, three sections from the substantia nigra pars compacta (anterior–posterior −2.92 mm, −3.28 mm and −3.64 mm from bregma, according to the mouse brain atlas by Franklin and Paxinos, 2008) and three sections from the striatum (anterior–posterior −1.10 mm, 0.74 mm and 0.38 mm from bregma) were analysed. CD11b immunostaining was evaluated with the Scion Image analysis program (Scion Corp.). Inside each frame, the area occupied by grey values above the threshold was automatically calculated. For each level of the substantia nigra pars compacta or striatum the obtained value was first normalized with respect to vehicle, and the values from the different levels were then averaged. For GFAP analysis, in the substantia nigra pars compacta and striatum, the mean number of GFAP-positive cells obtained from each experimental group was first normalized with respect to vehicle and the values from the different levels were then averaged.

α-Synuclein extraction

Twenty milligrams of brain tissue were homogenized in five volumes of Tris-buffered saline plus (TBS^+) buffer (Tris–HCl 50 mM pH 7.4, NaCl 175 mM, EDTA 5 mM, PMSF 0.1 mM and *N*-ethylmaleimide 1 mM; Sigma) using a glass homogenizer on ice. The homogenate was centrifuged at 120 000 *g* for 30 min at 4°C. The supernatant (S1) was saved, and the pellet was dissolved in TBS^+ buffer with

1% Triton^{TM} X-100 and centrifuged at 120 000 *g* for 30 min at 4°C to obtain the second supernatant (S2). The procedure was repeated, the supernatant (S3) was retained and the pellet was dissolved in urea 8 M (SIGMA) with SDS 5% to obtain the supernatant S4.

Immunoblot analysis

To analyse the tissue level of soluble α-synuclein, supernatants S1, S2 and S3 were loaded into SDS–PAGE gels and analysed by western blot technique. S4 supernatants were analysed to detect insoluble α-synuclein. Briefly, protein extracts were diluted in loading buffer (Sigma) and boiled for 2 min before being loaded into an SDS–PAGE gel and transferred to a nitrocellulose membrane (Amersham). Membranes were then incubated with either α-synuclein (1:500; BD) or monoclonal anti-β-actin (1:10 000; Sigma) primary antibody and secondary antibodies coupled to horseradish peroxidase (1:1500, Santa Cruz Biotechnology). Immunopositive bands were visualized by enhanced chemiluminescence detection (ECL) reagents (Amersham).

DMT1 immunoreactivity was examined in total mesencephalic and striatal extracts by using a pan-DMT1 antibody (Santa Cruz Biotechnology). The levels of dopamine transporter were analysed in striatal extracts using the anti-dopamine transporter rat monoclonal antibody (Santa Cruz Biotechnology 1:200). Gel analysis was performed using the NIH ImageJ free software (web link http://rsbweb.nih.gov/ij/).

High-performance liquid chromatography assays

Striatal tissue was sonicated in 250 µl of 0.2 M perchloric acid and centrifuged at 11 000 *g* for 15 min at 4°C. The supernatant was filtered (0.45 µm) and diluted 1:62.5. Twenty microlitres were injected into an HPLC with a reverse-phase column [LC-18 DB, 15 cm, 5-µm particle size and a coulometric detector (ESA Coulochem II)] to quantify monoamines and their metabolites. For dopamine and noradrenaline (NA), the mobile phase was: NaH_2PO_4, 100 mM; Na_2EDTA, 0.1 mM; *N*-octyl sodium sulphate, 0.5 mM; 7.5% methanol; pH 5.5. For 5-hydroxytryptamine, 5-hydroxyindoleacetic acid, dihydroxylphenylacetic acid and homovanillic acid, the mobile phase was: CH_3COONa, 0.23 M; citric acid, 0.15 M; Na_2EDTA, 100 mg/ml; 6.5% methanol; pH: 4.7. The sensitivity of the assay was 10 fmol/sample. The values of these monoamines are expressed as picomoles/gram wet weight of tissue.

Behavioural studies

Motor activity assessment

Spontaneous motility was assessed in a quiet isolated room. Mice were placed individually in plexiglass cages (length 47 cm, height 19 cm, width 27 cm) with a metal grid over the floor and equipped with infrared photocell emitters-detectors situated along the long axis of each cage (Opto-Varimex Mini; Columbus Instruments). The interruption of a photocell beam was detected by a counter that recorded the total number of photocell beam interruptions. The counter recorded two different types of motor activity: locomotor activity due to the locomotion of the mouse along the axes of the cage and total motor activity due to locomotion plus non-finalized movements (stereotyped behaviours such as grooming, rearing, and sniffing). The counter recognized the stereotyped movements because of the continuous interruption of the same photocell beam, whereas locomotion along the cage produced interruptions of different photocell beams. Motor activity counts were evaluated for 60 min. Spontaneous locomotor activity was further investigated and expressed as distance travelled by using an automated video tracking system (EthoVision XT, Noldus Information Technology) in a 45 × 45 cm cage, with walls of clear acrylic poly(methyl methacrylate) (Phenotyper mod. 4500, Noldus). On this occasion, PhenoTyper was used as a basic cage for a short period of time (1 h). Locomotor activity was also evaluated using the PhenoTyper home cages (Noldus Information Technology) under a reversed light:dark cycle (white light: 20:00–8:00 h, red light: 8:00–20:00 h), with food and water available *ad libitum*. One animal per cage was analysed for six consecutive days with 24 h of automated monitoring. The principal parameter analysed was the total distance moved (cm) in a day.

CatWalk gait analysis

Gait parameters were evaluated using the CatWalk® 7.1 system (Noldus). All data analyses were performed with a pixel threshold value ⩾25 arbitrary units. Mice were subjected to 3 days of training before the test. Mice were trained to cross the walkway (30 min/day) and were rewarded after every successful continuous run with highly palatable food. Animals were subjected to a food restriction protocol consisting of a diet of 1.5 g/day of standard laboratory chow. Water was available *ad libitum*. Testing was performed on Day 4 when the animals completed three runs without hesitation, and parameters such as base of support, print length, maximum contact at (%) and swing speed were measured. The weight of the animals was monitored during all the experiments.

L-DOPA treatment

L-DOPA (L-3,4-dihydroxyphenylalanine methyl ester hydrochloride) and benserazide hydrochloride were purchased from Sigma Aldrich and freshly dissolved in a saline solution at a final injection volume of 5 ml/kg. Both L-DOPA (20 mg/kg) and benserazide hydrochloride (12.5 mg/kg) or vehicle (saline) were injected intraperitoneally into mice 1 h before the beginning of the behavioural tests.

Locomotor activity was individually measured as described above. Briefly, the animals were singularly placed in a novel PhenoTyper cage and spontaneous locomotor activity was video-recorded. Videos were then analysed by Ethovision XT software. For the CatWalk gait analysis, trained mice were treated with L-DOPA and tested as described above.

Statistical analysis

Statistical analysis was performed with the GraphPad Prism 4.0 program. Comparisons between two groups were performed using the two-tailed unpaired Student's *t*-test. Data were expressed as the mean ± SEM. Statistical significance was accepted at the 95% confidence level ($P < 0.05$).

The variations in monoamines and their metabolites were evaluated by a one-way ANOVA followed by Tukey's *post hoc* test.

Motor activity was evaluated using a one-way ANOVA followed by the Newman-Keuls *post hoc* test. Performance in the PhenoTyper cages was evaluated with a two-tailed unpaired Student's *t*-test. Statistical significance was accepted at the 95% confidence level ($P < 0.05$). For the analysis of gait parameters, the means of the hind and front paws were considered. The individual averages for each mouse were calculated over three runs, and the differences between groups were evaluated with a two-tailed unpaired Student's *t*-test. Statistical significance was accepted at the 95% confidence level ($P < 0.05$).

Results

Dopaminergic neuronal loss in the substantia nigra pars compacta of 18-month-old c-rel$^{-/-}$ mice

We studied possible occurrence of age-related neurodegeneration in the substantia nigra pars compacta of c-rel$^{-/-}$ mice.

The quantification of substantia nigra pars compacta dopaminergic cell bodies and their projecting fibres in the striatum was performed using tyrosine hydroxylase immunostaining. Our results showed a significant loss of dopaminergic neurons in the substantia nigra pars compacta of c-rel$^{-/-}$ mice with ageing. Indeed, 18-month-old mice displayed a ~40% reduction in dopaminergic neurons compared with wild-type mice (c-rel$^{-/-}$ 4671 ± 239, wild-type 7569 ± 316; $P < 0.05$; Fig. 1G–I). No decrease in dopaminergic neurons was detected in 2-month-old c-rel$^{-/-}$ mice (Fig. 1A–C) (c-rel$^{-/-}$ 7289 ± 322, wild-type 6905 ± 380; $P > 0.05$) or 12-month-old animals (Fig. 1D–F) (c-rel$^{-/-}$ 7801 ± 407, wild-type 7720 ± 395; $P > 0.05$). Remarkably, the loss of tyrosine hydroxylase-positive neurons in 18-month-old c-rel$^{-/-}$ mice paralleled the total loss of Nissl-stained cells (c-rel$^{-/-}$ 9809 ± 558, wild-type 13397 ± 620; $P < 0.05$) in the substantia nigra pars compacta, suggesting that dopaminergic neuron survival and not simply tyrosine hydroxylase expression was diminished in the brains of aged c-rel$^{-/-}$ mice (Fig. 1L–N). No significant change in the estimated number of Nissl-stained cells was evident in the substantia nigra pars compacta of 2- and 12-month-old c-rel$^{-/-}$ mice compared with age-matched controls (data not shown).

Neurons of ventral tegmental area, medial septal area, nucleus basalis magnocellularis and striatum are spared from degeneration in aged c-rel$^{-/-}$ mice

With the aim to investigate other brain regions possibly undergoing age-related degeneration, we evaluated the survival of dopaminergic neurons in the ventral tegmental area and of cholinergic

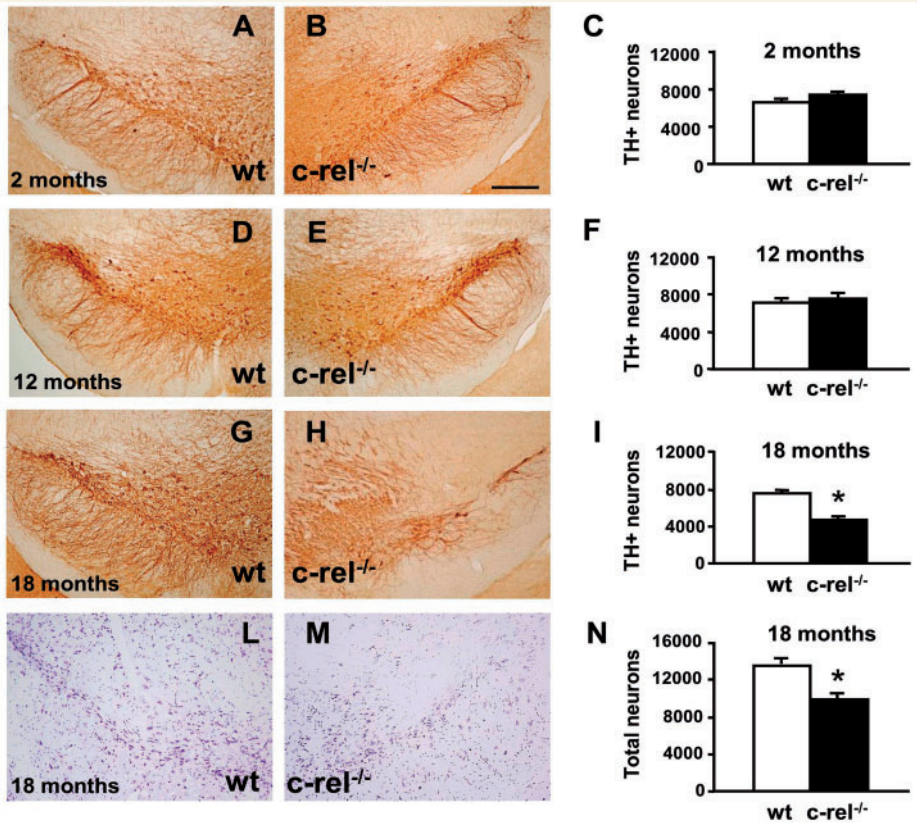

Figure 1 Age-dependent loss of dopaminergic neurons in the substantia nigra of c-rel$^{-/-}$ mice. Representative pictures of tyrosine hydroxylase staining in the substantia nigra dopaminergic neurons of wild-type and c-rel$^{-/-}$ mice at 2 months (**A** and **B**), 12 months (**D** and **E**) and 18 months (**G** and **H**). The data from stereology analysis of tyrosine hydroxylase-positive cells are shown in **C**, **F** and **I**. A significant decrease of the number of tyrosine hydroxylase-positive neurons was detected in 18-month-old c-rel$^{-/-}$ mice. The data represent the means ± SEM ($n = 8$ mice/group, $^*P < 0.05$ versus wild-type mice). Representative pictures of Nissl staining in the substantia nigra of 18-month-old wild-type (**L**) and c-rel$^{-/-}$ mice (**M**) confirmed the loss of neurons. Data from stereology analysis are reported in **N**. Scale bar in **B** = 350 μm and applies to **A**–**M**. TH = tyrosine hydroxylase.

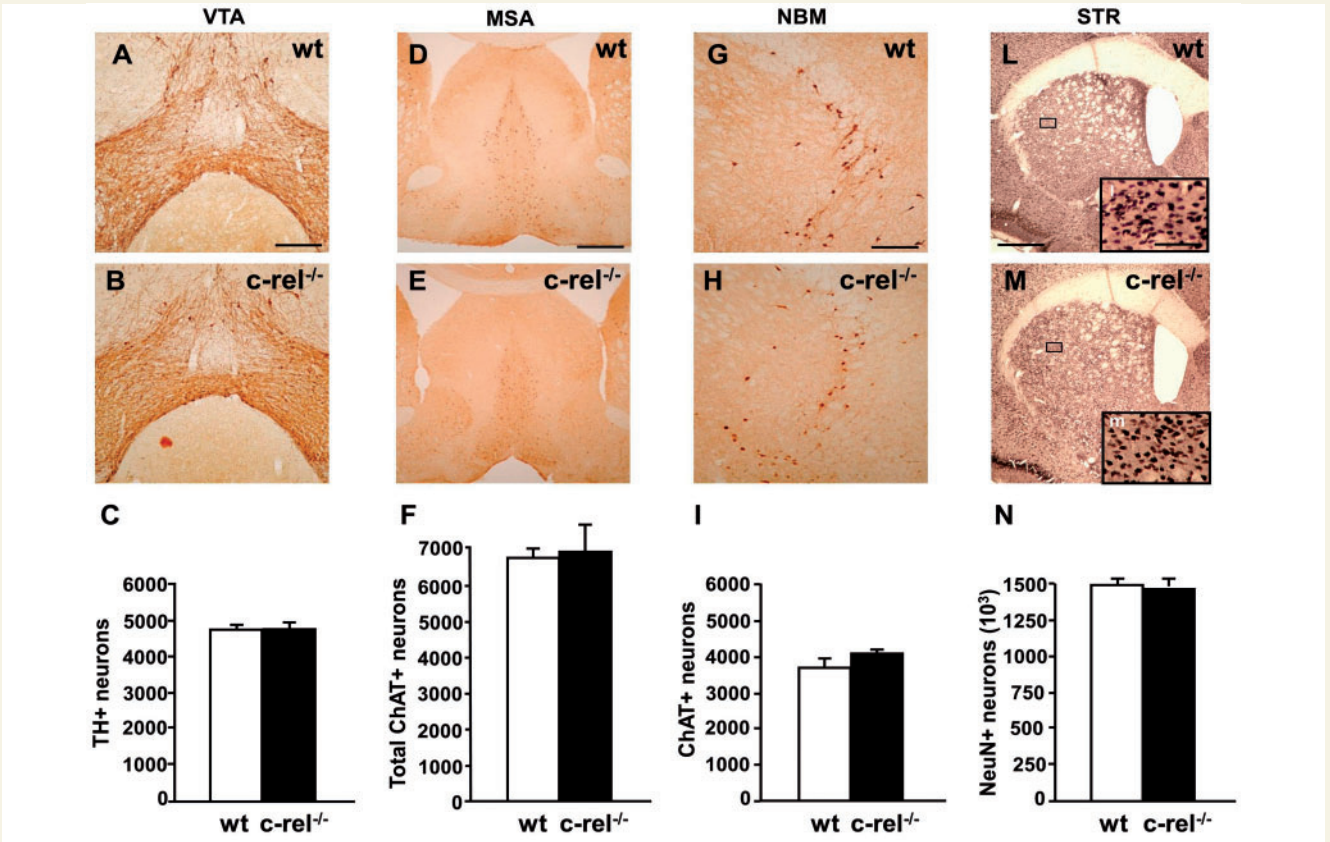

Figure 2 Tyrosine hydroxylase staining in the ventral tegmental area, ChAT staining in the medial septal area and nucleus basalis magnocellularis, NeuN staining in the striatum, of 18-month-old mice. Representative photomicrographs of tyrosine hydroxylase staining in the ventral tegmental area of wild-type (**A**) and c-rel$^{-/-}$ (**B**) mice. (**C**) Densitometry analysis of tyrosine hydroxylase-positive cells. No significant decrease in tyrosine hydroxylase-positive neurons was evident in c-rel$^{-/-}$ mice. The data represent the mean ± SEM ($n = 7$ animals per group, $^*P < 0.05$ versus wild-type mice). Representative photomicrographs are shown of ChAT staining in the medial septal area of wild-type (**D**) and c-rel$^{-/-}$ mice (**E**) and in the nucleus basalis magnocellularis of wild-type (**G**) and c-rel$^{-/-}$ (**H**) animals. Representative pictures of NeuN staining in the striatum of wild-type (**L**) and c-rel$^{-/-}$ (**M**) mice. No significant difference in the estimated number of ChAT-positive cells in the medial septal area (**F**) and the nucleus basalis magnocellularis (**I**) or NeuN-positive neurons in the striatum (**N**) was evident between the two groups. Data represent the means ± SEM ($n = 6$ animals per group, $^*P < 0.05$ versus wild-type mice). Scale bars: in **A** = 350 μm for **A** and **B**; in **D** = 500 μm for **D** and **E**; in **G** = 350 μm for **G** and **H**; **L** = 1200 μm for **L–M**, l insert = 300 μm for **l**, **m**. MSA = medial septal area; NBM = nucleus basalis magnocellularis; STR = striatum; VTA = ventral tegmental area; wt = wild-type.

cells in the medial septal area and nucleus basalis magnocellularis. No change in the number of tyrosine hydroxylase-positive neurons in the ventral tegmental area of c-rel$^{-/-}$ mice was detected either at 2 (data not shown) or 18 months (Fig. 2A–C). Likewise, no significant difference in the ChAT-positive cholinergic neurons was found in the medial septal area (Fig. 2D–F) and the nucleus basalis magnocellularis (Fig. 2G–I) of c-rel$^{-/-}$ mice at 18 months or 2 months (data not shown). We also evaluated a possible loss of striatal neurons in c-rel$^{-/-}$ mice. No difference in the estimated number of NeuN-positive neurons was detected in 18-month-old (Fig. 2L–N) and 2-month-old (data not shown) c-rel$^{-/-}$ mice.

Loss of dopaminergic terminals in the striatum

To determine whether the loss of dopaminergic neurons in the substantia nigra pars compacta of c-rel$^{-/-}$ mice was associated with a reduction in the number of nigrostriatal projections, we quantified tyrosine hydroxylase-positive nerve terminals in the dorsal striatum. Our experiments showed a reduction of ~50% of the area occupied by tyrosine hydroxylase-positive fibres in the striatum of 18-month-old c-rel$^{-/-}$ mice (Fig. 3A–E).

As a marker of dopaminergic terminals, we also evaluated striatal dopamine transporter levels in 18-month-old control and knockout mice. In parallel with the loss of tyrosine hydroxylase-positive fibres, western blot analysis (Fig. 3F) showed a marked decrease in dopamine transporter immunoreactivity in c-rel$^{-/-}$ mice with respect to wild-type mice. To corroborate the dopaminergic terminal loss in the striatum of 18-month-old c-rel$^{-/-}$ mice we investigated the occurrence of neurochemical changes by measuring dopamine and dopamine metabolites in whole striata using HPLC (Fig. 3G). Dopamine and homovanillic acid levels appeared significantly decreased in c-rel$^{-/-}$ mice when compared with

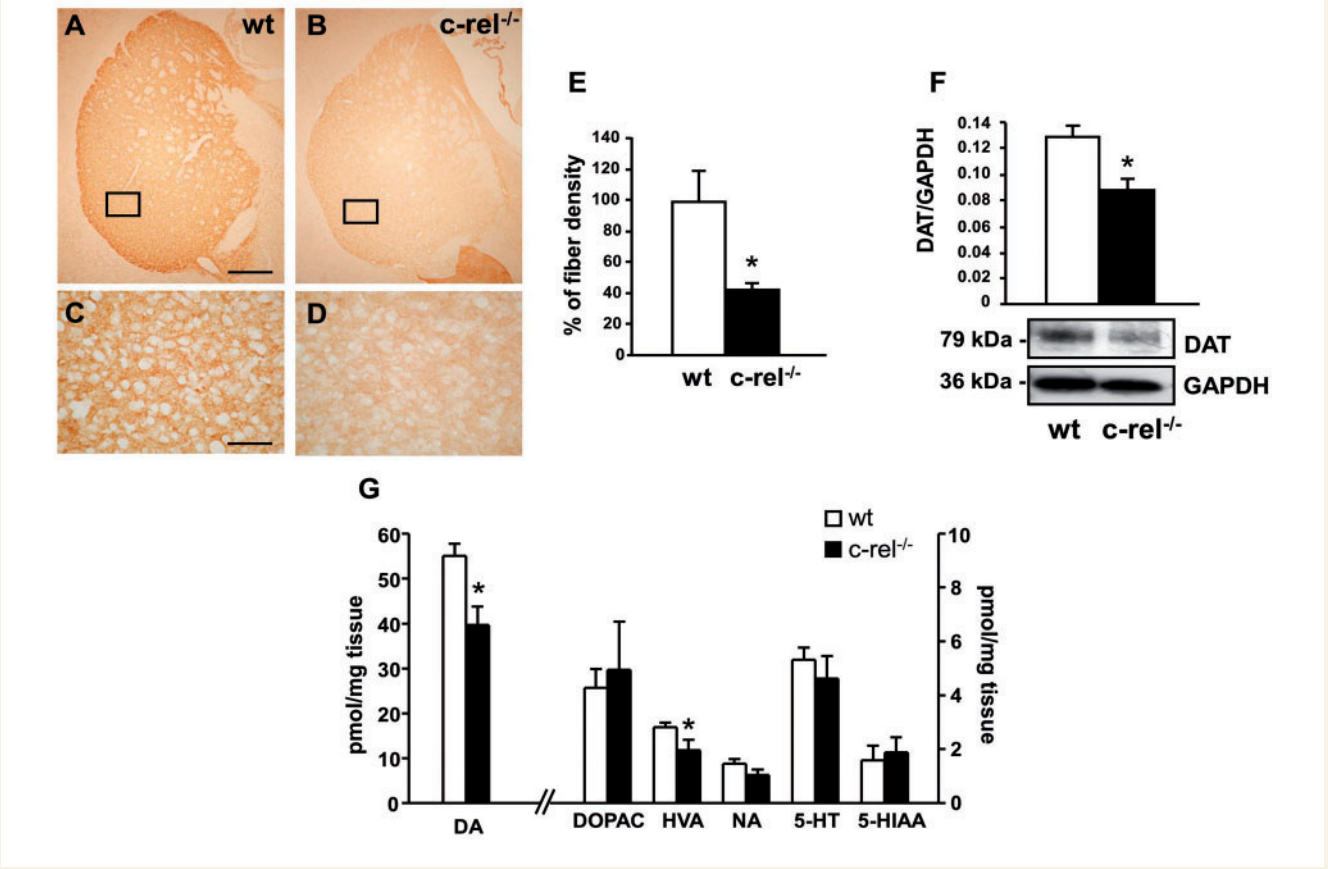

Figure 3 Molecular changes in the dorsal striatum. Low (**A** and **B**) and high magnification (**C** and **D**) of representative pictures of tyrosine hydroxylase immunostaining in caudate putamen sections from 18-month-old wild-type (**A–C**) and c-rel$^{-/-}$ mice (**B–D**). (**E**) Densitometric analysis revealed a significant decrease in the density of tyrosine hydroxylase-positive fibres in 18-month-old c-rel$^{-/-}$ mice. The data represent the mean ± SEM ($n = 4$ animals per group, $^*P < 0.05$ versus wild-type mice). Scale bar in **A** = 500 μm for **A** and **B**; in **C** = 300 μm for **C** and **D**. (**F**) Representative immunoblotting of the dopamine transporter in the caudate putamen extracts of 18-month-old wild-type and c-rel$^{-/-}$ mice. Densitometry analysis showed a significant reduction in dopamine transporter levels in c-rel$^{-/-}$ when compared with wild-type animals. Results represent the mean ± SEM ($n = 4$ animals per group, $^*P < 0.05$ versus wild-type mice). (**G**) Quantification of dopamine, dopamine metabolites (dihydroxylphenylacetic acid and homovanillic acid), NA, 5-hydroxytryptamine with relative metabolite (5-hydroxyindoleacetic acid) detected in caudate putamen extracts of 18-month-old mice by HPLC analysis. A significant decrease of dopamine and homovanillic acid levels was detected in c-rel$^{-/-}$ mice. Data are means ± SEM of three independent experiments ($n = 5$ animals for group. $^*P < 0.05$ versus wild-type mice). Quantification of noradrenaline, dopamine with its metabolites (homovanillic acid and dihydroxylphenylacetic acid) and 5-hydroxytryptamine with its metabolite (5-hydroxyindoleacetic acid) detected in the caudate putamen extracts of 18-month-old mice by HPLC analysis. A significant decrease in dopamine and homovanillic acid levels was detected in c-rel$^{-/-}$ mice. Data represent the mean ± SEM of three independent experiments ($n = 5$ animals per group, $^*P < 0.05$ versus wild-type mice). DA = dopamine; DAT = dopamine transporter; DOPAC = dihydroxylphenylacetic acid; HVA = homovanillic acid; 5HT = 5-hydroxytryptamine; 5HIAA = 5-hydroxyindoleacetic acid; NA = noradrenaline.

wild-type animals, whereas dihydroxylphenylacetic acid levels were unchanged. The dihydroxylphenylacetic acid:dopamine ratio displayed a trend to increase that did not reach statistical significance (data not shown), indicating that only a minor up-regulation of dopamine turnover can occur in the nigro-striatal terminals of aged c-rel$^{-/-}$ mice. No significant difference in the levels of noradrenaline, 5-hydroxytryptamine and its metabolite 5-hydroxyindoleacetic acid was evident between wild-type and c-rel$^{-/-}$ mice.

Accumulation of soluble and aggregated α-synuclein and increase of DMT1 level in the mesencephalon of 18-month-old c-rel$^{-/-}$ mice

After identifying dopaminergic neuronal loss in substantia nigra pars compacta of c-rel$^{-/-}$ mice at 18 months, we evaluated specific markers associated with Parkinson's disease at this time

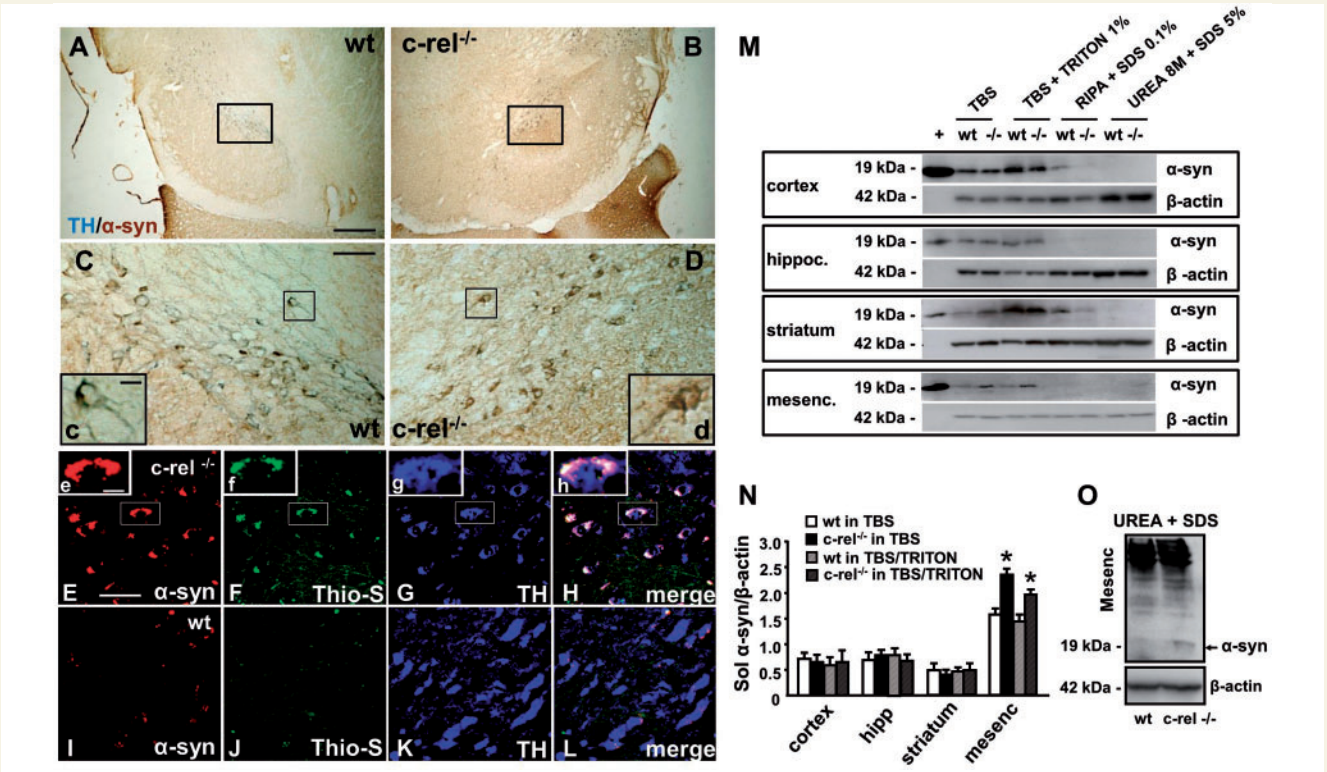

Figure 4 Accumulation of α-synuclein in 18-month-old c-rel$^{-/-}$ and wild-type mice. (**A** and **D**) Representative photomicrographs showing tyrosine hydroxylase (blue) and α-synuclein (brown) double staining in the substantia nigra of 18-month-old wild-type (**A** and **C**) and c-rel$^{-/-}$ mice (**B** and **D**). Note that the increase of brown α-synuclein staining in the c-rel$^{-/-}$ mice (**d**) completely covered the blue tyrosine hydroxylase immunoreactivity observed in wild-type mice (**c**). (**E-L**) Representative photomicrographs showing α-synuclein (red), thioflavin S (green) and tyrosine hydroxylase (blue) triple staining in the substatia nigra of c-rel$^{-/-}$ (**E–H**) and wild-type (**I–L**) mice. Note that the α-synuclein-positive aggregates in the brain of c-rel$^{-/-}$ mice were also thioflavin S immunopositive, as visualized in the high-magnification squares in panels **E–H**. Scale bars: in **A** = 3 mm for **A** and **B**; in **C** = 750 μm for **C** and **D**; in insert c = 10 μm for **c** and **d**; in E = 50 μm for **E–L**; in insert e = 10 μm for **e–h**. Panels **A–L** are representative of three independent experiments (n = 3 animals per group). (**M**) Representative western blot showing sequential α-synuclein extraction from diverse brain areas in 18-month-old wild-type and c-rel$^{-/-}$ (-/-) mice. Recombinant α-synuclein (+) solution was used as positive control. Note the increase in α-synuclein-immunopositive bands in the mesencephalon of c-rel$^{-/-}$ mice when compared with wild-type animals, as well as the α-synuclein immunopositive band in the urea extracts from c-rel$^{-/-}$ mice. (**N**) Densitometric analysis of α-synuclein-immunopositive bands in the TBS and TBS/Triton fractions. Note the significant increase of α-synuclein in the mesencephalon of c-rel$^{-/-}$ mice. Data represent the mean ± SEM (n = 3 animals per group, *P < 0.05 versus wild-type mice). (**O**) Representative western blot showing the increase in the α-synuclein immunoreactive bands in the urea + SDS fractions from the mesencephalon of c-rel$^{-/-}$ mice. Similar results were obtained in three separate experiments.

point. Lewy bodies, eosinophilic inclusions mainly composed of filamentous α-synuclein aggregates, are among the typical pathological hallmarks of Parkinson's disease. Hence, we studied whether c-rel$^{-/-}$ mice might display pathological deposition of α-synuclein. We found that c-rel$^{-/-}$ mice showed specific immunoreactivity for α-synuclein with the degeneration of dopaminergic neurons in the substantia nigra pars compacta. A strong α-synuclein immunoreactivity (brown staining) indicative of protein accumulation, was visible within tyrosine hydroxylase-positive neurons (blue staining) of c-rel$^{-/-}$ mice (Fig. 4B, D and inset d). Conversely, a weak α-synuclein immunoreactivity was present within tyrosine hydroxylase-positive neurons of wild-type animals (Fig. 4A, C and inset c). The α-synuclein-positive inclusions in the dopaminergic neurons of the substantia nigra pars compacta were thioflavin S-positive (Fig. 4F, H and insets f and h), indicating that α-synuclein protein was aggregated in a pathological fibrillary form in c-rel$^{-/-}$ mice.

The content of α-synuclein sequentially extracted from the mesencephalon, cortex, striatum and hippocampus of mice was evaluated by western blot analysis (Fig. 4M–O). These extractions were sequentially carried out in TBS^{+}, TBS^{+} and 1% Triton^{TM} X-100, and RIPA buffer for the isolation of the soluble form of α-synuclein and in 8 M urea/5% SDS to collect the insoluble fraction. We detected an accumulation of native α-synuclein protein in the mesencephalon of c-rel$^{-/-}$ mice when compared with wild-type animals, but no significant change in the protein content of other brain regions (cortex, striatum and hippocampus) (Fig. 4M). Levels of soluble α-synuclein in the TBS^{+} and TBS^{+} with 1% Triton^{TM} X-100 fractions were quantified by densitometric analysis. A statistically significant increase of soluble α-synuclein

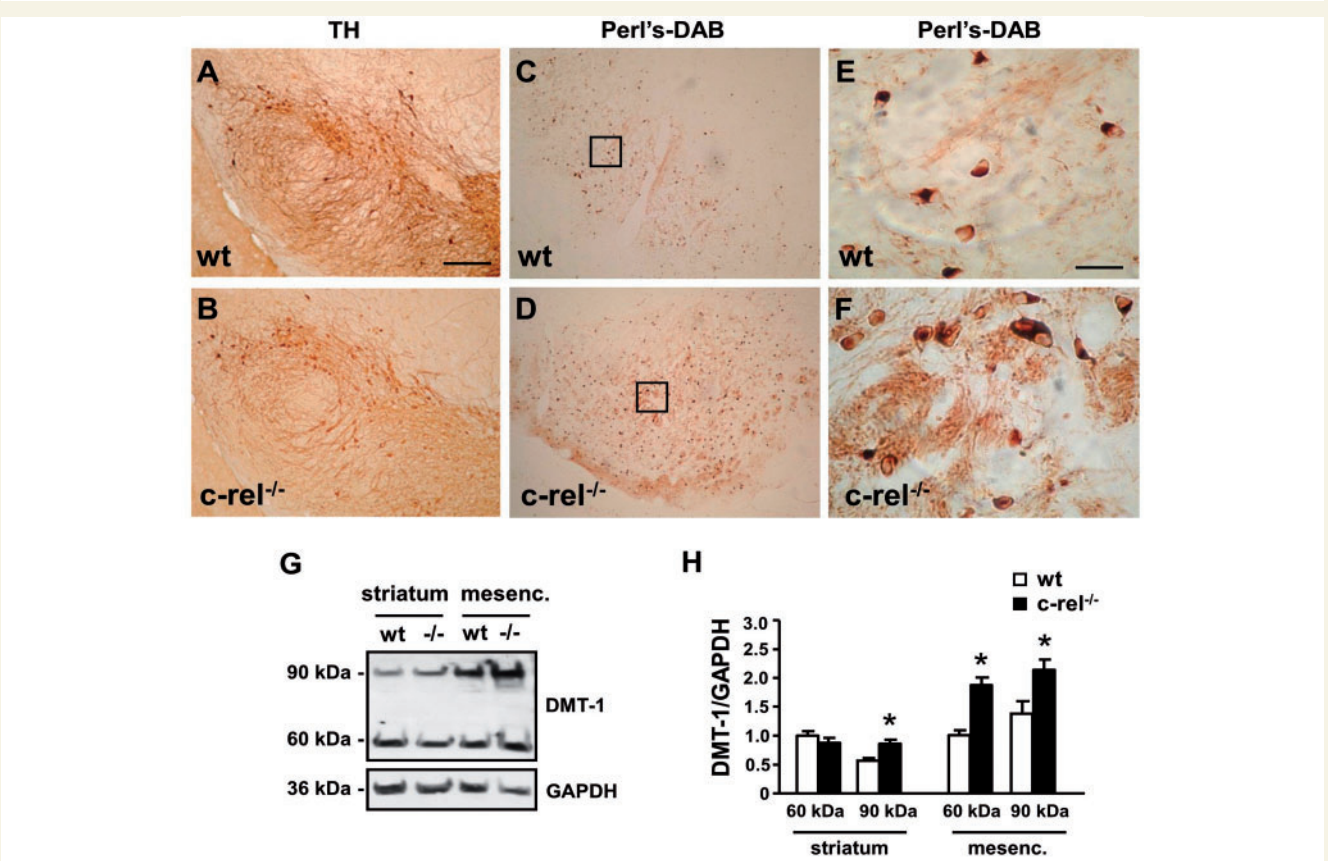

Figure 5 DMT1 immunoreactivity and iron staining in mesencephalon of 18-month-old c-rel$^{-/-}$ and wild-type mice. Tyrosine hydroxylase staining (**A** and **B**) and diaminobenzidine enhanced Perl iron staining (**C–F**) in sections of 18-month-old wild-type (**A, C** and **E**) and c-rel$^{-/-}$ mice (**B, D** and **F**). Higher magnifications of Perl iron staining are in panels **E** and **F**. While the number of tyrosine hydroxylase-positive neurons decreased, the iron staining significantly increased in the substantia nigra pars compacta and reticulata of c-rel$^{-/-}$ mice compared with wild-type mice. Representative immunoblotting of the ferrous iron transporter DMT1 in the striatal and mesencephalic extracts of 18-month-old wild-type and c-rel$^{-/-}$ mice (**G**). Densitometric analysis of DMT1 relative to GAPDH (**H**). DMT1 60 and 90 kDa bands significantly increased in the mesencephalon of c-rel$^{-/-}$ mice (-/-) compared with wild-type animals. Significant difference in the DMT1 90 kDa band was detected in the striatum. Values represent the mean ± SEM ($n = 3$ animals per group, $^{*}P < 0.001$ versus wild-type mice) (**F**). Scale bar in A = 600 μm for **A–D**; in E = 75 μm for **E** and **F**.

levels was detected in the mesencephalon of c-rel$^{-/-}$ mice when compared with wild-type mice (Fig. 4N). Accumulation of insoluble α-synuclein in the mesencephalon was confirmed by the presence of a 19-kDa α-synuclein-immunopositive band in the urea/SDS extracts of aged c-rel$^{-/-}$ mice but not in wild-type animals (Fig. 4M and O).

As a further indication of the occurrence of Parkinson's disease-like pathological changes in the substantia nigra pars compacta of c-rel$^{-/-}$ mice, we measured DMT1 levels and iron staining. Western blot analysis by anti-DMT1 antibody revealed a significant increase of the differently glycosylated 60 and 90 kDa DMT1 components in the mesencephalic extracts of 18-month-old c-rel$^{-/-}$ mice. An increase in the 90 kDa component was detected in striatal extracts (Fig. 5G and H). Also, we found an elevation of iron levels by diaminobenzidene-enhanced Perl staining in the substantia nigra pars compacta of 18-month-old c-rel$^{-/-}$ mice as compared with the wild-type animals. A greater number of iron-positive cells were evident along the entire substantia nigra pars compacta formation (Fig. 5A–F).

Microglia activation in substantia nigra pars compacta and striatum of 18-month-old c-rel$^{-/-}$ mice

To assess whether the age-related degeneration of substantia nigra pars compacta dopaminergic cells in c-rel$^{-/-}$ mice is accompanied by glial activation as described in Parkinson's disease brain we investigated microglial and astroglial morphology in the substantia nigra pars compacta and striatum. Compared with aged-matched wild-type animals, 18-month-old c-rel$^{-/-}$ mice displayed marked microglial activation, as revealed by CD11b immunostaining in the striatum and substantia nigra pars compacta (Fig. 6A–D). The presence of microglial activation in the substantia nigra pars compacta and striatum of c-rel$^{-/-}$ mice was confirmed by the quantification of the CD11b-immunopositive area (Fig. 6E). Analysis of GFAP immunostaining revealed the presence of protoplasmic astrocytes that remained non-reactive in the substantia nigra pars compacta and striatum of c-rel$^{-/-}$ mice (Fig. 6F–L).

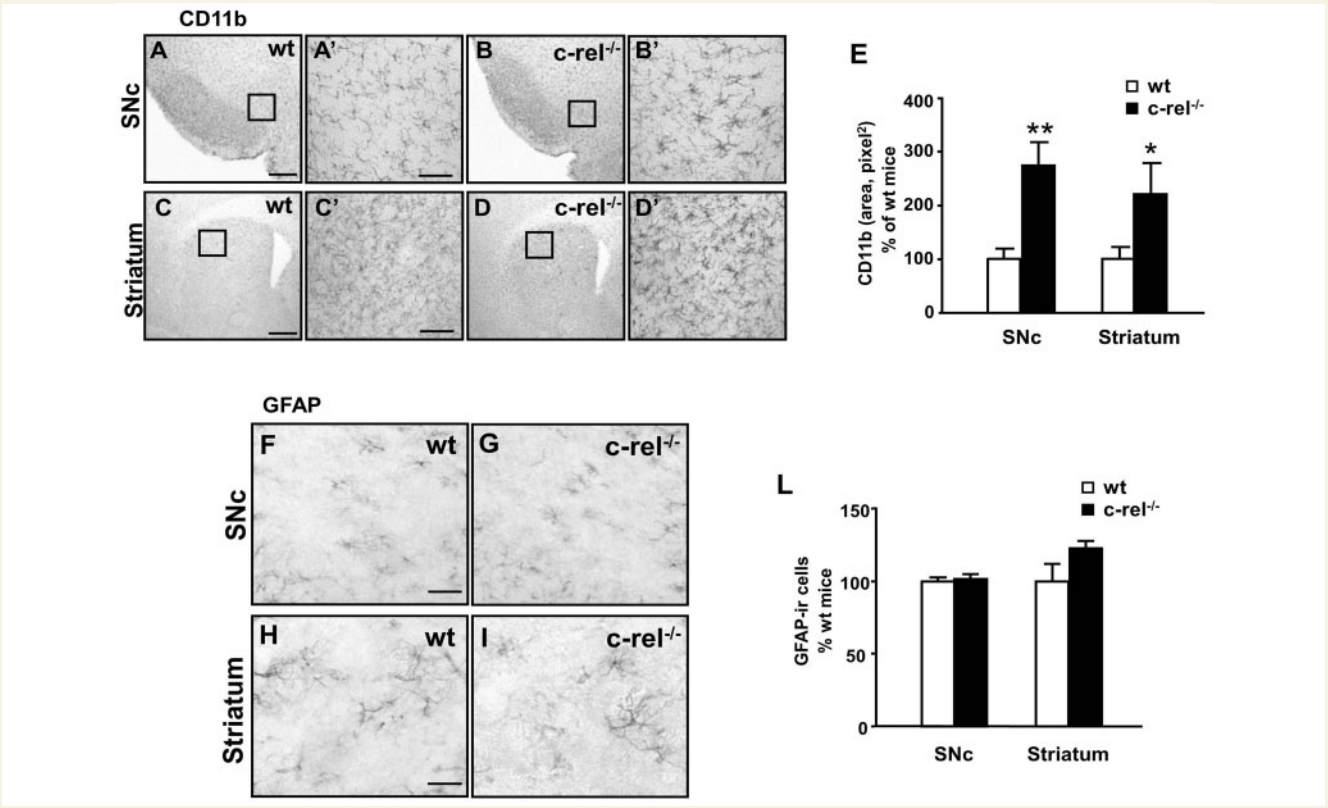

Figure 6 CD11b and GFAP immunoreactivity in 18-month-old c-rel$^{-/-}$ and wild-type mice. Pictures of the substantia nigra pars compacta (**A** and **B**) and striatum (**C** and **D**) sections from 18-month-old wild-type (**A** and **C**) and c-rel$^{-/-}$ mice (**B** and **D**) illustrating CD11b microglial immunostaining. (**E**) The quantification of CD11b is expressed as a percentage of grey values. There was significant microglial activation in both the striatum and the substantia nigra pars compacta of c-rel$^{-/-}$ mice. Images of the substantia nigra pars compacta (**F** and **G**) and striatum (**H** and **I**) sections from 18-month-old wild-type (**F** and **H**) and c-rel$^{-/-}$ mice (**G** and **I**) showing GFAP astroglial immunostaining. (**L**) The percentage of GFAP-positive cells. No evident changes in astroglial activation were found in c-rel$^{-/-}$ mice. Scale bars: in **A** = 200 μm for **A–D**; in **C'** and **F** = 50 μm for **A'–D'** and **F–I**. Data represent the mean ± SEM ($n = 5$ animals per group, $^{*}P < 0.05$, $^{**}P < 0.005$ versus wild-type mice). SNc = sunstantia nigra pars compacta.

Behavioural evaluation

Three separate groups of either c-rel$^{-/-}$ or wild-type mice at 4, 12 and 18 months of age were tested for their spontaneous motor behaviour. Motor activity was evaluated as total activity and locomotor activity during 60 min of observation in photobeam cages recording the number of photocell beam interruptions. At 4 or 12 months of age, no significant difference was found in the spontaneous motor and locomotor activity between the two groups (Fig. 7A and B). In contrast, at 18 months, both the total and the spontaneous locomotor activity appeared to be reduced in c-rel$^{-/-}$ mice (Fig. 7C). Locomotor activity was also evaluated in 1-h video-tracking observations of individual mice in PhenoTyper cages, allowing an accurate determination of total distance moved. Our observations confirmed that the total distance covered by c-rel$^{-/-}$ mice was significantly lower than that moved by wild-type mice (Fig. 7D). Locomotor performance was then continuously monitored for 6 days in the PhenoTyper, which allowed home-cage evaluation of locomotor activity, unaffected by anxiety. The total distance moved on Days 5 and 6 was significantly lower for c-rel$^{-/-}$ mice compared with the wild-type group (Fig. 7E).

Wild-type and c-rel$^{-/-}$ mice were tested for their spontaneous gait behaviour (Fig. 8). No significant differences in weight were observed within or between the experimental groups. Gating of c-rel$^{-/-}$ mice was affected: in particular, c-rel$^{-/-}$ mice displayed a lower swing speed (limb velocity when the paw is not in contact with the ground) (Fig. 8A) and a wider distance between left and right front-paws or hind-paws (base of support) (Fig. 8B and C). Furthermore, c-rel$^{-/-}$ mice needed a longer time to reach the max contact (per cent of time spent to reach the maximal paw/floor contact area, relative to the total time spent in contact with the floor; Fig. 8D) and displayed a lower forepaw print length (Fig. 8E) when compared with wild-type animals (Fig. 8F).

L-DOPA supplementation reverses motor deficits

The effect of dopamine replacement was tested by treating c-Rel-deficient mice with L-DOPA (20 mg/kg) combined with benserazide hydrochloride (12.5 mg/kg) or vehicle, 1 h before the beginning of the behavioural tests. The acute L-DOPA administration

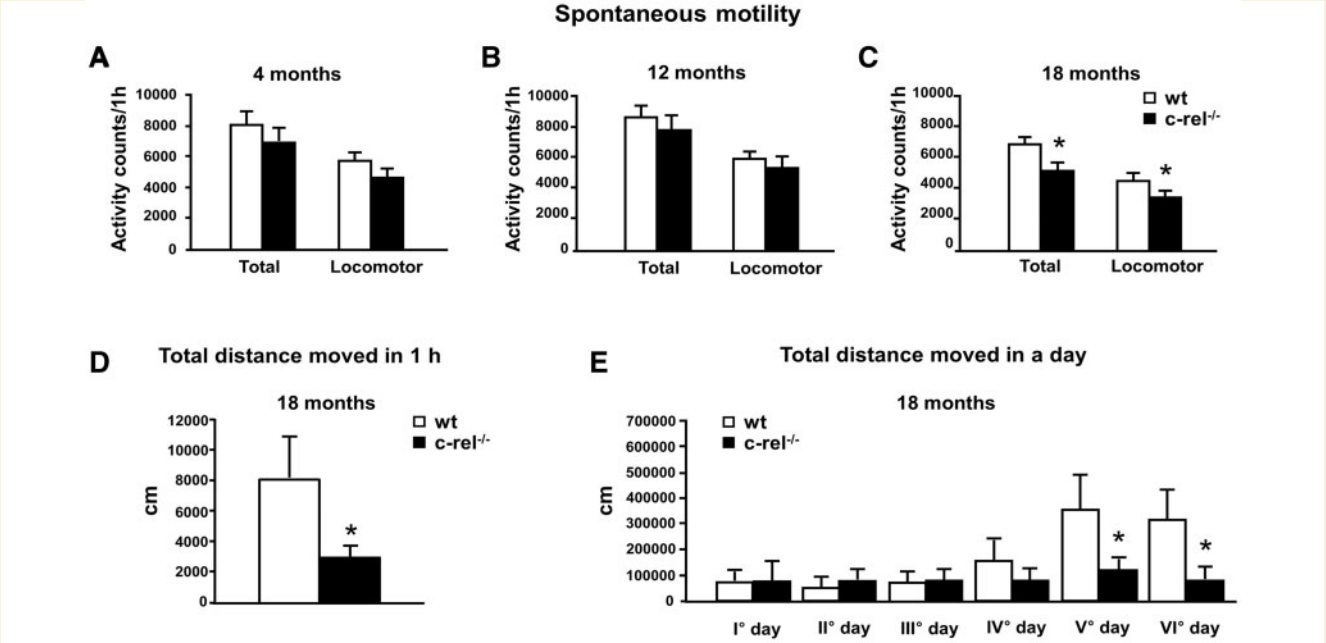

Figure 7 Spontaneous motor and locomotor activity in c-rel$^{-/-}$ and wild-type mice. (**A–C**) Mice were tested at 4 months (**A**, $n = 9–10$), 12 months (**B**, $n = 17–18$) and 18 months (**C**, $n = 14–18$). The data represent the mean ± SEM of the total motor and locomotor activity counts registered during the 60-min observation (*$P < 0.05$ versus wild-type mice). (**D**) Mice at 18 months were tested by a video-tracking system in a open field arena for 1 h. c-rel$^{-/-}$ mice were less active as assessed by the total distance moved (cm) ($n = 6$ animals per group, *$P < 0.05$ versus wild-type mice). (**E**) The wild-type and c-rel$^{-/-}$ mice at 18 months were maintained in a PhenoTyper cage and continuously monitored for six consecutive days. The total distance moved (cm) in a day increased after 4 days of observation in the wild-type group but not in the c-rel$^{-/-}$ group ($n = 11$ animals per group, *$P < 0.05$ versus wild-type mice).

significantly reversed the hypomotility of c-rel$^{-/-}$ mice. The distance moved by the L-DOPA treated group during a 1 h observation was twice longer than that moved by vehicle-treated mice (Fig. 9A). L-DOPA administration did not significantly modify the locomotor activity in wild-type mice (data not shown).

Furthermore, L-DOPA supplementation reversed most of the deficits in the gait-related parameters in trained c-rel$^{-/-}$ mice. Swing speed significantly increased (Fig. 9B) while the bases of support (Fig. 9C and D) and the time to maximal contact (Fig. 9E) significantly decreased. The print length tended to increase in mice treated with L-DOPA (Fig. 9E).

Discussion

This study shows that mice carrying a knockout of NFκB c-Rel factor developed a Parkinson's disease-like phenotype with ageing that makes them a suitable model for this disorder. Eighteen-month-old c-rel$^{-/-}$ mice displayed a selective loss of tyrosine hydroxylase-positive neurons in the substantia nigra pars compacta with accumulation of aggregated α-synuclein, iron with DMT1 and reduced dopamine content in the striatum. Moreover, they developed age-dependent deficits in motor performance that were reversed by acute L-DOPA supplementation. Although a lot of effort has been devoted to studying Parkinson's disease pathophysiology, the mechanisms underlying the onset and progression of the disease are still unclear, largely due to the lack of animal models that reproduce the origin and symptoms of Parkinsonian syndromes. The widely used models based on the administration of neurotoxins do not include any genetic predisposition. They show a rapid degeneration of dopaminergic neurons that does not reproduce the multifactorial, slow and progressive changes occurring in human disease (Tieu, 2011). The toxin-based models highly contributed to the development of palliative therapies, though their use has not led to successful disease-modifying therapies for Parkinson's disease. Since a large panel of genes is related to the onset of familial forms of Parkinson's disease (Bekris *et al*., 2010), several genetic models have been developed, though they only partially recapitulate certain aspects of the disease (Chesselet and Richter, 2011).

It has been hypothesized that brain trauma may represent a risk factors for the development of Parkinson's disease via the induction of apoptotic biochemical cascades (Mattson and Camandola, 2001; Hutson *et al.*, 2011). Among the mechanisms that control neuronal survival in neurodegenerative diseases, the activation of NFκB transcription factors is one of the most prominent (Mattson and Camandola, 2001). Interestingly, in patients with Parkinson's disease the proportion of substantia nigra pars compacta dopaminergic neurons with immunoreactive RelA in their nuclei was found to be >70-fold that in controls (Hunot *et al*., 1997). Sustained RelA activation has been found in mesencephalic astrocytes and microglial cells of patients with Parkinson's disease and 1-methyl-4-phenyl-1,2,3,6-tetrahydropyridine (MPTP)-treated mice. Remarkably, treatment with the IκB kinase inhibitor,

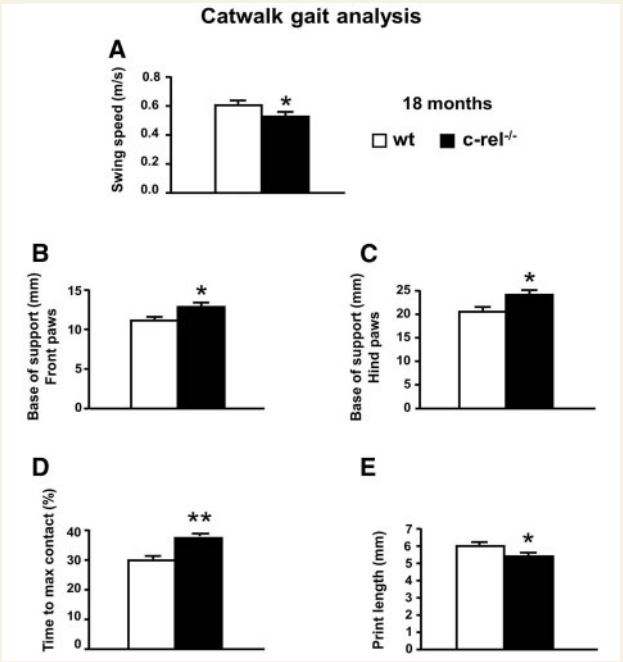

Figure 8 CatWalk gait analysis of c-rel$^{-/-}$ and wild-type mice. The data represent the mean ± SEM of three runs per animal ($n = 11$ animals per group). (**A**) Lower swing speed (m/s) and higher base of support for both the front (**B**) and hind (**C**) paws was observed in c-rel$^{-/-}$ mice (*$P < 0.05$ versus wild-type mice). Higher percentage of time spent to reach the maximum contact (**D**) of the front limbs was observed in c-rel$^{-/-}$ mice (**$P < 0.001$ versus wild-type mice). A lower print length of the front paws (**E**) was observed in c-rel$^{-/-}$ mice (*$P < 0.05$ versus wild-type mice).

NEMO-binding domain peptide, inhibited RelA activation and counteracted the onset of microgliosis and neurodegeneration in mice exposed to MPTP (Ghosh *et al*., 2007). This would support the hypothesis that the activation of NFκB RelA is a key event in neurodegeneration (Pizzi *et al*., 2002, 2005; Inta *et al*., 2006; Sarnico *et al*., 2009). Conversely, NFκB containing the c-rel subunit has been shown to prevent neuronal apoptosis in experimental models of stroke and Alzheimer's disease (Pizzi *et al*., 2002, 2005; Sarnico *et al*., 2009; Valerio *et al*., 2009) as well as in models of 1-methyl-4-phenylpyridinium (MPP+)-induced neurotoxicity (Sarnico *et al*., 2008).

Our working hypothesis was that due to the altered balance between RelA- and c-Rel-mediated effects on neuron vulnerability, mice carrying a knockout of the c-rel gene might develop pathological brain alterations. c-Rel$^{-/-}$ mice had normal brain development and conserved good health during their lifetime. However, at 18 months of age, these mice exhibited a ~40% loss of dopaminergic neurons in the substantia nigra pars compacta, as assessed by tyrosine hydroxylase-immunoreactivity and Nissl staining. No degeneration of dopamine neurons was detected in the ventral tegmental area, a dopaminergic region commonly spared in Parkinson's disease (Dauer and Przedborski, 2003). Likewise, there was no evident loss of cholinergic neurons in the nucleus basalis magnocellularis and medial septal area of the basal forebrain or in striatal neurons.

Mice carrying the c-Rel deficiency developed a significant loss of nigral dopaminergic terminals in the striatum, as shown by the reduced density of tyrosine hydroxylase-positive fibres and a lower dopamine transporter protein level. There was lower striatal concentration of dopamine and homovanillic acid, but no changes

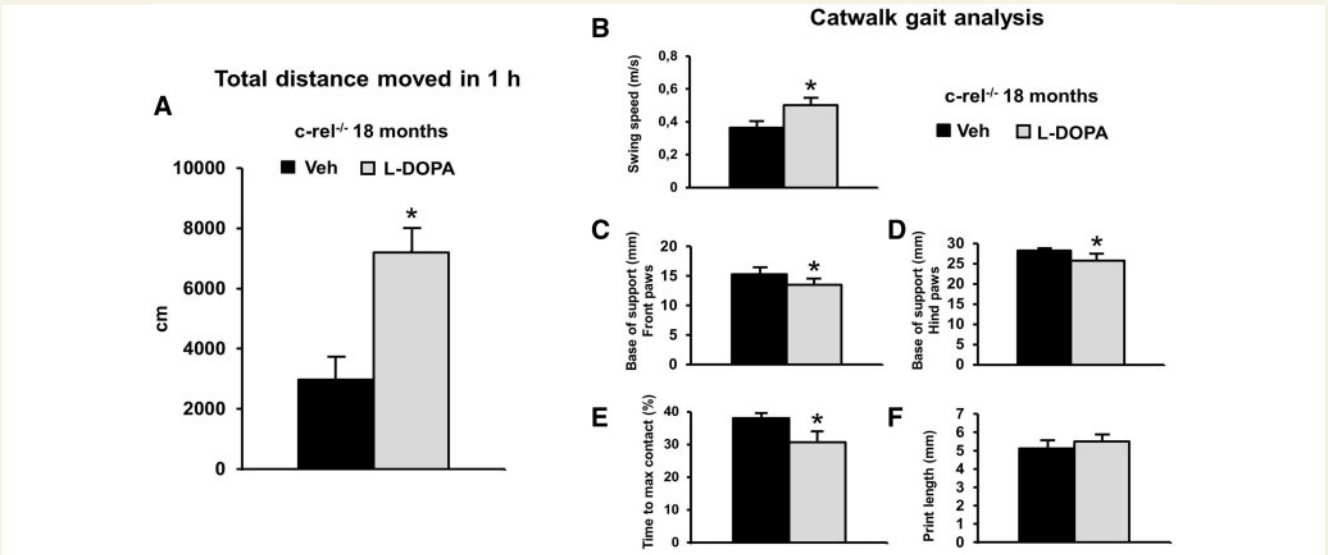

Figure 9 L-DOPA treatment ameliorates the motor deficits in c-rel$^{-/-}$ mice (18 months). L-DOPA (20 mg/kg) and benserazide hydrochloride (12.5 mg/kg), or vehicle, were administered to mice 1 h before the beginning of the behavioural tests. (**A**) L-DOPA treatment increased the spontaneous locomotor activity evaluated as total distance moved (cm) in the open field during 1 h observation (*$P < 0.05$ versus vehicle). L-DOPA supplementation improved the gaiting performance by increasing the swing speed (m/s) (**B**), by reducing the base of support for both the front (**C**) and hind paws (**D**) and by reducing the percentage of time spent to reach the maximum contact (**E**) (*$P < 0.05$ versus vehicle). L-DOPA treatment increased, though not significantly, the fore paw print length (mm) (**F**). veh = vehicle. The data represent the mean ± SEM of three runs per animal ($n = 6$ animals per group).

in noradrenaline, 5-hydroxytryptamine or 5-hydroxyindoleacetic acid levels, illustrating the selective degeneration of nigral dopamine neurons in these mice. Interestingly, dihydroxylphenylacetic acid did not significantly decrease. Dopamine is metabolized to dihydroxylphenylacetic acid and 3-methoxytyramine through monoamine oxidase and catechol-*O*-methyl transferase, respectively, and both are converted to homovanillic acid, as final metabolite (Elsworth and Roth, 1997). A decrease of homovanillic acid in the CSF is actually considered a biomarker for patients with Parkinson's disease (LeWitt, 2012). Even if monoamine oxidase B is located at the mitochondrial outer membrane in both neurons and glial cells, a large portion of extracellular dihydroxylphenylacetic acid may derive from the metabolism of intraneuronal dopamine pool (Meissner *et al*., 2003). Catechol-*O*-methyl transferase, however, is located extraneuronally both in glial cells and postsynaptic membranes (Elsworth and Roth, 1997). Consistent with the significant decrease in dopamine transporter and tyrosine hydroxylase-positive terminals in the striatum of c-rel$^{-/-}$ mice, lower homovanillic acid levels probably reflect a decrease in the amount of released dopamine, rather than a decrease of newly synthesized dopamine in striatal terminals. Indeed, the absence of dihydroxylphenylacetic acid changes may even reflect increased dopamine synthesis in the spared terminals to partially compensate for the loss of dopamine striatal innervation, as seen in both asymptomatic and symptomatic Parkinson's disease primate models (Pifl and Hornykiewicz, 2006).

These neurochemical changes were accompanied by the onset of motor deficits. Impairments in locomotor and total motor activity were evident in c-rel$^{-/-}$ mice at 18 months of age, but not in younger mice, as previously observed (O'Ryordan *et al*., 2006; Ahn *et al*., 2008). The spontaneous locomotor activity was particularly affected, as aged c-rel$^{-/-}$ mice travelled ~70% less distance in 1 h. We also recorded motor activity for six consecutive days using a video-based observation system in the PhenoTyper cages, to avoid stress-related biases. In our setup conditions, wild-type mice moved little during the first 4 days of habituation and were more explorative after the fifth day of habituation. In contrast, c-rel$^{-/-}$ mice displayed constantly lower locomotor activity. Although we cannot exclude that exploratory activity might also be reduced from this test, additional gaiting analysis supported the presence of locomotor dysfunctions in 18-month-old c-rel$^{-/-}$ mice. Similarly to other Parkinson's disease rat models (Vlamings *et al*., 2007; Chuang *et al*., 2010; Vandeputte *et al*., 2010), 18-month-old c-rel$^{-/-}$ mice showed changes in several gait-related parameters. They had a lower swing speed, i.e. the speed at which the paw moves while in mid-air. In addition, c-rel$^{-/-}$ mice spent a longer time to reach the maximum contact area of front limb paws with the glass. Notably, both swing speed and max contact area were related to bradykinesia (Koopmans *et al*., 2007) and were observed in rats with bilateral (Vlamings *et al*., 2007) and unilateral (Chuang *et al*., 2010) 6-hydroxydopamine lesion. Static parameters were also affected in c-rel$^{-/-}$ mice, as the distance between controlateral footprints of knockout animals increased compared to wild-type mice, indicating a peculiar posture modification. Posture modifications, such as widely spread hind toes, were previously reported in MTPT-treated mouse models of Parkinson's disease (Rozas *et al*., 1998). Furthermore, forelimb print length was reduced in c-rel$^{-/-}$ mice suggesting that they had dysfunctional paw extensions and coordination. All these changes might be related to reduced paw pressure during paw contact, a phenomenon that may be related to muscle tone rigidity and altered use of paw surface, as suggested by Chuang *et al*. (2010).

c-Rel-deficient mice were found to model key relevant features of Parkinson's disease including responsiveness to L-DOPA, that is diagnostic of Parkinson's disease (Lees, 1986). Indeed, treatment with L-DOPA plus benserazide, a peripheral aromatic amino acid decarboxylase inhibitor, reversed the deficit in locomotor activity of c-rel$^{-/-}$ mice evaluated through measuring the distance travelled in 1 h. Moreover, L-DOPA treatment significantly improved all gait-related deficits in c-rel$^{-/-}$ mice, with the exclusion of print length which, however, tended to recover.

Further pathological examination of aged c-rel$^{-/-}$ brains showed marked immunoreactivity for α-synuclein, which accumulated in the spared dopaminergic neurons of the substantia nigra pars compacta. These intracellular aggregates were stained with thioflavin S, indicating the presence of fibrillary α-synuclein. The immunoblot analysis confirmed the accumulation of soluble α-synuclein in the mesencephalon of c-rel$^{-/-}$ mice, but not in the cortex, hippocampus, or striatum. Remarkably, we also detected urea/SDS insoluble α-synuclein in the mesencephalon of 18-month-old c-rel$^{-/-}$ mice. α-Synuclein deposition is considered a central pathological event for the onset and progression of Parkinson's disease (Braak *et al*., 2003; Uversky *et al*., 2007; Bellucci *et al*., in press) as α-synuclein gene mutations and multiplications are responsible for developing familial forms of Parkinson's disease with classical brain histopathology (Bekris *et al*., 2010). Experimental evidence suggests that α-synuclein may induce neuronal degeneration via multiple mechanisms (Uversky *et al*., 2007; Bellucci *et al*., in press), but whether α-synuclein aggregation is the primary cause or an epiphenomenon in the pathogenic process of Parkinson's disease has yet to be established.

The presence of neuroinflammatory markers, including activated microglial and astrocytic cells, is another important neuropathological feature of Parkinson's disease brain (Hirsch and Hunot 2009). Studies in experimental models of Parkinson's disease suggest that microglia activation and up-regulation of inflammatory mediators can both be induced by α-synuclein and may contribute to the pathogenesis of the disease (Zhang *et al*., 2005). Studies examining astrocyte response in the substantia nigra pars compacta of patients with Parkinson's disease showed variable results (Forno *et al*., 1992; Damier *et al*., 1993; Mirza *et al*., 2000; Song *et al*., 2009) and the role of astrocytes in Parkinson's disease initiation and progress is debated (Hirsch and Hunot 2009; Chung *et al*., 2010). We observed a marked microglia activation in the substantia nigra pars compacta and striatum but no GFAP-positive astrocytic reaction in 18-month-old c-rel$^{-/-}$ mouse brains. This may either reflect an early stage of neuroinflammation in the brain of c-rel$^{-/-}$ mice or an effect associated with the lack of c-Rel-mediated transcription, which needs to be investigated.

A remarkable increase in iron content, together with lower physiological iron scavenger ferritin, is also present in the

substantia nigra pars compacta of patients with Parkinson's disease (Sian-Hülsmann *et al*., 2010). The cerebral iron accumulation has been associated with local enhancement of the Fenton reaction generating reactive oxygen species and α-synuclein fibril formation (Uversky *et al*., 2007; Sian-Hülsmann *et al*., 2010). In mice treated with MPTP, iron increases were correlated with the selective degeneration of substantia nigra pars compacta dopaminergic neurons (Lv *et al*., 2011). Moreover, recent studies reported increases of iron and DMT1 in glia and neuromelanin-positive neurons of patients with Parkinson's disease and demonstrated a link between DMT1 up-regulation and substantia nigra pars compacta degeneration in animal models of Parkinson's disease (Salazar *et al*., 2008; Lv *et al*., 2011). Consistently with their ability to develop a Parkinson's disease-like phenotype, 18-month-old c-rel$^{-/-}$ mice displayed increased amounts of both the 60 and 90 kDa forms of DMT1 in the mesencephalon and striatum, in conjunction with increased iron staining in the substantia nigra pars compacta.

Understanding the pathogenesis of Parkinson's disease-like neurodegeneration in aged c-rel$^{-/-}$ mice needs further detailed investigation. Emerging evidence indicates that the selective vulnerability of substantia nigra pars compacta neurons in Parkinson's disease depends on the peculiar 'energy-demanding' physiology of these cells (Surmeier *et al*., 2011). Substantia nigra pars compacta dopaminergic neurons display an enormous axonal field and a number of synapses for each axon that is orders of magnitude higher than that of other neurons (Arbuthnott and Wickens 2007). Moreover, during their pacemaking activity, substantia nigra pars compacta dopaminergic neurons generate autonomous action potentials by unusual engaging of L-type Ca^{2+} channels that require subsequent activation of ATP-dependent Ca^{2+} pumps to maintain proper cytoplasmic Ca^{2+} homeostasis (Wilson and Callaway, 2000). Notably, Ca^{2+}-dependent pacemaking and secondary generation of oxidative stress were observed in substantia nigra pars compacta dopaminergic cells, but not in ventral tegmental area neurons resistant to Parkinson's disease (Guzman *et al*., 2010). To afford the conspicuous energy demand, mitochondria and endoplasmic reticulum in substantia nigra pars compacta dopaminergic neurons generate amounts of reactive oxygen species which are constantly neutralized by antioxidant systems including super oxide dismutases (MnSOD and copper and zinc SOD), catalases, and the glutathione peroxidase (Halliwell, 2006). Activation of UCP4 and UCP5, the brain-specific isoforms of *UCP*, also contribute to reducing the reactive oxygen species generation and reactive oxygen species-mediated toxicity (Kwok *et al*., 2010; Ho *et al*., in press). Interestingly, knocking-out DJ1 (*PARK7*), a gene associated with an early-onset form of Parkinson's disease, downregulated the expression of *UCP4* and *UCP5* and increased the oxidation of matrix proteins in substantia nigra pars compacta dopaminergic neurons, but not in the ventral tegmental area (Gutzman *et al*., 2010). All this evidence suggests that sensitizing genetic backgrounds and environmental challenges could easily synergize with the intrinsic stress of substantia nigra pars compacta dopaminergic neurons to exacerbate cellular damage, ageing, and ultimately death (Surmeier *et al*., 2011).

Notably, c-Rel factor is a transcriptional inducer of UCP4 (Ho *et al*., in press), MnSOD (Bernard *et al*., 2001; Pizzi *et al*., 2005) and anti-apoptotic Bcl-xL (Chen *et al*., 2000; Sarnico *et al*., 2009). It can be hypothesized that reduced expression of UCP4 and MnSOD in c-Rel-deficient mice might enhance reactive oxygen species accumulation occurring with ageing in substantia nigra pars compacta neurons (Cardozo-Pelaez *et al*., 1999). It is also feasible that this oxidative stress may contribute to elevate intracellular levels of α-synuclein (Uversky *et al*., 2007), DMT1 and iron (Salazar *et al*., 2008) and, in turn, may lead to α-synuclein aggregation (Uversky *et al*., 2007), microglia activation and neuronal damage (Zhang *et al*., 2005). Reduced Bcl-xL expression, by lessening the resilience of substantia nigra pars compacta dopaminergic neurons to the vicious cycle of oxidative stressors and α-synuclein aggregation, would finally hasten cell death and the development of motor deficits. A comprehensive evaluation of mitochondrial function and transcriptional profiles in substantia nigra pars compacta dopaminergic neurons of c-rel$^{-/-}$ mice could provide a validation of this hypothesis.

In conclusion, our data reveal a role for c-Rel factor as a regulator of substantia nigra pars compacta susceptibility to ageing. The specific pathology and loss of nigral dopaminergic neurons in aged c-rel$^{-/-}$ mice highlights the implications of c-Rel as a potential genetic risk factor for Parkinson's disease and a suitable molecular target for drug discovery.

Acknowledgements

We would like to thank Marina Bentivoglio for the thoughtful discussion of this study.

Funding

This work was supported by PRIN 2008; Ex 60% 2008–2011 University of Brescia; NEDD Project, (CUP H81J09002660007), Regione Lombardia, Italy; Parkinson's UK.

References

Ahn HJ, Hernandez CM, Levenson JM, Lubin FD, Liou HC, Sweatt JD. c-Rel, an NF-kappaB family transcription factor, is required for hippocampal long-term synaptic plasticity and memory formation. Learn Mem 2008; 15: 539–49.

Arbuthnott GW, Wickens J. Space, time and dopamine. Trends Neurosci 2007; 30: 62–9.

Bekris LM, Mata IF, Zabetian CP. The genetics of Parkinson disease. J Geriatr Psychiatry Neurol 2010; 23: 228–42.

Bellucci A, Zaltieri M, Navarria L, Grigoletto J, Missale C, Spano P. From α-synuclein to synaptic dysfunctions: new insights into the pathophysiology of Parkinson's disease. Brain Res 2012. In press.

Bernard D, Quatannens B, Begue A, Vandenbunder B, Abbadie C. Antiproliferative and antiapoptotic effects of crel may occur within the same cells via the up-regulation of manganese superoxide dismutase. Cancer Res 2001; 61: 2656–64.

Bethea JR, Castro M, Keane RW, Lee TT, Dietrich WD, Yezierski RP. Traumatic spinal cord injury induces nuclear factor-kappaB activation. J Neurosci 1998; 18: 3251–60.

Braak H, Del TK, Rub U, de Vos RA, Jansen Steur EN, Braak E. Staging of brain pathology related to sporadic Parkinson's disease. Neurobiol Aging 2003; 24: 197–211.

Camandola S, Mattson MP. NF-kappa B as a therapeutic target in neurodegenerative diseases. Expert Opin Ther Targets 2007; 11: 123–32.
Cardozo-Pelaez F, Song S, Parthasarathy A, Hazzi C, Naidu K, Sanchez-Ramos J. Oxidative DNA damage in the aging mouse brain. Mov Disord 1999; 14: 972–80.
Chen C, Edelstein LC, Gélinas C. The Rel/NF-kappaB family directly activates expression of the apoptosis inhibitor Bcl-x(L). Mol Cell Biol 2000; 20: 2687–95.
Chesselet MF, Richter F. Modelling of Parkinson's disease in mice. Lancet Neurol 2011; 10: 1108–18.
Chuang CS, Su HL, Cheng FC, Hsu SH, Chuang CF, Liu CS. Quantitative evaluation of motor function before and after engraftment of dopaminergic neurons in a rat model of Parkinson's disease. J Biomed Sci 2010; 17: 9.
Chung YC, Ko HW, Bok E, Park ES, Huh SH, Nam JH, et al. The role of neuroinflammation on the pathogenesis of Parkinson's disease. BMB Rep 2010; 43: 225–32.
Damier P, Hirsch EC, Zhang P, Agid Y, Javoy-Agid F. Glutathione peroxidase, glial cells and Parkinson's disease. Neuroscience 1993; 52: 1–6.
Dauer W, Przedborski S. Parkinson's disease: mechanisms and models. Neuron 2003; 39: 889–909.
Echtay KS. Mitochondrial uncoupling proteins–what is their physiological role? Free Radic Biol Med 2007; 43: 1351–71.
Elsworth JD, Roth RH. Dopamine synthesis, uptake, metabolism, and receptors: relevance to gene therapy of Parkinson's disease. Exp Neurol 1997; 144: 4–9.
Fahn S. Description of Parkinson's disease as a clinical syndrome. Ann N Y Acad Sci 2003; 991: 1–14.
Forno LS, DeLanney LE, Irwin I, Di Monte D, Langston JW. Astrocytes and Parkinson's disease. Prog Brain Res 1992; 94: 429–36.
Franklin K, Paxinos G. The mouse brain in Stereotaxic Coordinates, Compact 2nd edn. San Diego, CA: Academic Press; 2008.
Ghosh A, Roy A, Liu X, Kordower JH, Mufson EJ, Hartley DM, et al. Selective inhibition of NF-kappaB activation prevents dopaminergic neuronal loss in a mouse model of Parkinson's disease. Proc Natl Acad Sci USA 2007; 104: 18754–59.
Guzman JN, Sanchez-Padilla J, Wokosin D, Kondapalli J, Ilijic E, Schumacker PT, et al. Oxidant stress evoked by pacemaking in dopaminergic neurons is attenuated by DJ-1. Nature 2010; 468: 696–700.
Halliwell B. Oxidative stress and neurodegeneration: where are we now? J Neurochem 2006; 97: 1634–58.
Hirsch EC, Hunot S. Neuroinflammation in Parkinson's disease: a target for neuroprotection? Lancet Neurol 2009; 8: 382–97.
Ho JW, Ho PW, Liu HF, So DH, Chan KH, Tse ZH, et al. UCP4 is a target effector of NF-κB c-Rel pro-survival pathway against oxidative stress. Free Radic Biol Med 2012; 53: 383–94.
Hunot S, Brugg B, Ricard D, Michel PP, Muriel MP, Ruberg M, et al. Nuclear translocation of NF-kappaB is increased in dopaminergic neurons of patients with parkinson disease. Proc Natl Acad Sci USA 1997; 94: 7531–36.
Hutson CB, Lazo CR, Mortazavi F, Giza CC, Hovda D, Chesselet MF. Traumatic brain injury in adult rats causes progressive nigrostriatal dopaminergic cell loss and enhanced vulnerability to the pesticide paraquat. J Neurotrauma 2011; 28: 1783–801.
Inta I, Paxian S, Maegele I, Zhang W, Pizzi M, Spano P, et al. Bim and Noxa are candidates to mediate the deleterious effect of the NF-kappa B subunit RelA in cerebral ischemia. J Neurosci 2006; 26: 12896–903.
Kaltschmidt B, Uherek M, Volk B, Baeuerle PA, Kaltschmidt C. Transcription factor NF-kappaB is activated in primary neurons by amyloid beta peptides and in neurons surrounding early plaques from patients with Alzheimer disease. Proc Natl Acad Sci USA 1997; 94: 2642–47.
King MA, Scotty N, Klein RL, Meyer EM. Particle detection, number estimation, and feature measurement in gene transfer studies: optical fractionator stereology integrated with digital image processing and analysis. Methods 2002; 28: 293–99.
Koopmans GC, Deumens R, Brook G, Gerver J, Honig WM, Hamers FP, et al. Strain and locomotor speed affect over-ground locomotion in intact rats. Physiol Behav 2007; 92: 993–1001.
Kwok KH, Ho PW, Chu AC, Ho JW, Liu HF, Yiu DC, et al. Mitochondrial UCP5 is neuroprotective by preserving mitochondrial membrane potential, ATP levels, and reducing oxidative stress in MPP+ and dopamine toxicity. Free Radic Biol Med 2010; 49: 1023–35.
Lees AJ. L-dopa treatment and Parkinson's disease. Q J Med 1986; 59: 535–47.
Levenson JM, Choi S, Lee SY, Cao YA, Ahn HJ, Worley KC, et al. A bioinformatics analysis of memory consolidation reveals involvement of the transcription factor c-rel. J Neurosci 2004; 24: 3933–43.
LeWitt P. Recent advances in CSF biomarkers for Parkinson's disease. Parkinsonism Relat Disord 2012; 18: S49–51.
Liou HC, Jin Z, Tumang J, Andjelic S, Smith KA, Liou ML. c-Rel is crucial for lymphocyte proliferation but dispensable for T cell effector function. Int Immunol 1999; 11: 361–71.
Lv Z, Jiang H, Xu H, Song N, Xie J. Increased iron levels correlate with the selective nigral dopaminergic neuron degeneration in Parkinson's disease. J Neural Transm 2011; 118: 361–9.
Mattson MP, Camandola S. NF-kappaB in neuronal plasticity and neurodegenerative disorders. J Clin Invest 2001; 107: 247–54.
Meissner W, Harnack D, Reese R, Paul G, Reum T, Ansorge M, et al. High-frequency stimulation of the subthalamic nucleus enhances striatal dopamine release and metabolism in rats. J Neurochem 2003; 85: 601–9.
Mirza B, Hadberg H, Thomsen P, Moos T. The absence of reactive astrocytosis is indicative of a unique inflammatory process in Parkinson's disease. Neuroscience 2000; 95: 425–32.
Olanow CW, Tatton WG. Etiology and pathogenesis of Parkinson's disease. Annu Rev Neurosci 1999; 22: 123–44.
O'Riordan KJ, Huang IC, Pizzi M, Spano P, Boroni F, Egli R, et al. Regulation of nuclear factor kappaB in the hippocampus by group I metabotropic glutamate receptors. J Neurosci 2006; 26: 4870–79.
Pifl C, Hornykiewicz O. Dopamine turnover is upregulated in the caudate/putamen of asymptomatic MPTP-treated rhesus monkeys. Neurochem Int 2006; 49: 519–24.
Pizzi M, Spano P. Distinct roles of diverse nuclear factor-kappaB complexes in neuropathological mechanisms. Eur J Pharmacol 2006; 545: 22–8.
Pizzi M, Goffi F, Boroni F, Benarese M, Perkins SE, et al. Opposing roles for NF-kappa B/Rel factors p65 and c-Rel in the modulation of neuron survival elicited by glutamate and interleukin-1beta. J Biol Chem 2002; 277: 20717–23.
Pizzi M, Sarnico I, Boroni F, Benarese M, Steimberg N, Mazzoleni G, et al. NF-kappaB factor c-Rel mediates neuroprotection elicited by mGlu5 receptor agonists against amyloid beta-peptide toxicity. Cell Death Differ 2005; 12: 761–72.
Rozas G, López-Martín E, Guerra MJ, Labandeira-García JL. The overall rod performance test in the MPTP-treated-mouse model of Parkinsonism. J Neurosci Methods 1998; 83: 165–75.
Salazar J, Mena N, Hunot S, Prigent A, Alvarez-Fisher D, Arredondo M, et al. Divalent metal transporter 1 (DMT1) contributes to neurodegeneration in animal models of Parkinson's disease. Proc Natl Acad Sci USA 2008; 105: 18578–83.
Sarnico I, Boroni F, Benarese M, Sigala S, Lanzillotta A, Battistin L, et al. Activation of NF-kappaB p65/c-Rel dimer is associated with neuroprotection elicited by mGlu5 receptor agonists against MPP(+) toxicity in SK-N-SH cells. J Neural Transm 2008; 115: 669–76.
Sarnico I, Lanzillotta A, Boroni F, Benarese M, Alghisi M, Schwaninger M, et al. NF-kappaB p50/RelA and c-Rel-containing dimers: opposite regulators of neuron vulnerability to ischaemia. J Neurochem 2009; 108: 475–85.
Schneider A, Martin-Villalba A, Weih F, Vogel J, Wirth T, Schwaninger M. NF-kappaB is activated and promotes cell death in focal cerebral ischemia. Nat Med 1999; 5: 554–9.
Sian-Hülsmann J, Mandel S, Youdim MB, Riederer P. The relevance of iron in the pathogenesis of Parkinson's disease. J Neurochem 2010; 118: 939–57.

Smith MA, Harris PL, Sayre LM, Perry G. Iron accumulation in Alzheimer disease is a source of redox-generated free radicals. Proc Natl Acad Sci USA 1997; 94: 9866–8.

Song YJ, Halliday GM, Holton JL, Lashley T, O'Sullivan SS, McCann H, et al. Degeneration in different parkinsonian syndromes relates to astrocyte type and astrocyte protein expression. J Neuropathol Exp Neurol 2009; 68: 1073–83.

Spillantini MG, Crowther RA, Jakes R, Hasegawa M, Goedert M. Alpha-Synuclein in filamentous inclusions of Lewy bodies from Parkinson's disease and dementia with lewy bodies. Proc Natl Acad Sci USA 1998; 95: 6469–73.

Surmeier DJ, Guzman JN, Sanchez-Padilla J, Schumacker PT. The role of calcium and mitochondrial oxidant stress in the loss of substantia nigra pars compacta dopaminergic neurons in Parkinson's disease. Neuroscience 2011; 198: 221–31.

Tieu K. A guide to neurotoxic animal models of Parkinson's disease. Cold Spring Harb Perspect Med 2011; 1: a009316.

Uversky VN. Neuropathology, biochemistry, and biophysics of alpha-synuclein aggregation. J Neurochem 2007; 103: 17–37.

Valerio A, Dossena M, Bertolotti P, Boroni F, Sarnico I, Faraco G, et al. Leptin is induced in the ischemic cerebral cortex and exerts neuroprotection through NF-kappaB/c-Rel-dependent transcription. Stroke 2009; 40: 610–7.

Vandeputte C, Taymans JM, Casteels C, Coun F, Ni Y, Van Laere K, et al. Automated quantitative gait analysis in animal models of movement disorders. BMC Neurosci 2010; 11: 92.

Vlamings R, Visser-Vandewalle V, Koopmans G, Joosten EA, Kozan R, Kaplan S, et al. High frequency stimulation of the subthalamic nucleus improves speed of locomotion but impairs forelimb movement in Parkinsonian rats. Neuroscience 2007; 148: 815–23.

Wilson CJ, Callaway JC. Coupled oscillator model of the dopaminergic neuron of the substantia nigra. J Neurophysiol 2000; 83: 3084–100.

Wirdefeldt K, Adami HO, Cole P, Trichopoulos D, Mandel J. Epidemiology and etiology of Parkinson's disease: a review of the evidence. Eur J Epidemiol 2011; 26: S1–58.

Zhang W, Wang T, Pei Z, Miller DS, Wu X, Block ML, et al. Aggregated alpha-synuclein activates microglia: a process leading to disease progression in Parkinson's disease. FASEB J 2005; 19: 533–42.